The Role of the Divergent Circulation for Large-Scale Eddy Momentum Transport in the Tropics. Part II: Dynamical Determinants of the Momentum Flux

PABLO ZURITA-GOTOR

Universidad Complutense de Madrid, and Instituto de Geociencia UCM-CSIC, Madrid, Spain

(Manuscript received 9 October 2018, in final form 5 February 2019)

ABSTRACT

This paper investigates the coupling between the rotational and divergent circulations aiming to explain the observations that show that the tropical eddy momentum flux is due to correlations between divergent eddy meridional velocities and rotational eddy zonal velocities. A simple linear model in which the observed eddy divergence field is used to force the vorticity equation can reproduce quite well the observed tropical eddy momentum flux. The eddy momentum flux in the model shows little sensitivity to the basic-state winds and is mainly determined by the characteristics of the divergent forcing. Vortex stretching and divergent advection of planetary vorticity produce eddy momentum flux contributions with the same sign but the former forcing dominates. It is shown that the main factor affecting the direction of the eddy momentum flux response to both forcings is the meridional tilt of the divergence phase lines, albeit with an opposite sign to the classical relation between rotational momentum flux and streamfunction phase tilt. How this divergent structure is determined remains an open question.

1. Introduction

Dima et al. (2005) noted that the observed climatological-mean stationary wave in the tropics bears a striking degree of hemispheric symmetry during both solstice seasons, in spite of the strong seasonality of the eddy forcing associated with the shift of the convective heating into the summer hemisphere. They proposed that the propagation of the eddies from the summer to the winter hemisphere might be important for setting up this symmetric pattern. Their hypothesis is supported by the strong seasonality of tropical eddy momentum fluxes, which are directed from the winter to the summer hemisphere (indicating propagation in the opposite direction for waves with westerly pseudomomentum) during both solstice seasons. This seasonal cross-equatorial propagation cancels out in the annual mean, producing much smaller annually averaged eddy momentum fluxes.

Despite its important impacts, the interhemispheric propagation of Rossby waves is not fully understood. Classical Rossby wave propagation theory (Hoskins and Karoly 1981) predicts no meridional propagation through boreal summer easterlies. During boreal winter, it has been argued that meridional propagation may be possible across westerly ducts, particularly over the eastern Pacific (Webster and Holton 1982; Hoskins and Ambrizzi 1993). However, the classical propagation conditions are modified in the presence of significant zonal-mean meridional flow (Schneider and Watterson 1984), a scenario of some relevance to the tropics due to the strong cross-equatorial Hadley cell. Li et al. (2015) show that this meridional flow plays an important role for interhemispheric Rossby wave propagation, consistent with the arguments of Schneider and Watterson (1984).

In a study very relevant to this work, Kraucunas and Hartmann (2007) used a simple shallow-water model to investigate what factors are important for the observed structure of the tropical climatological-mean stationary wave and the determination of the cross-equatorial eddy momentum flux. They found that the winter-hemisphere response to summer-hemisphere forcing is significantly enhanced by the Hadley cell flow, a sensitivity that they attributed to the impact of the mean meridional flow on propagation suggested by the work of Schneider and Watterson (1984). They also used a

Denotes content that is immediately available upon publication as open access.

Corresponding author: Pablo Zurita-Gotor, pzurita@alum.mit.edu

DOI: 10.1175/JAS-D-18-0304.1

simple barotropic, beta-plane model to illustrate this effect analytically.

However, because all these ideas on meridional propagation are based on the analysis of the barotropic or quasigeostrophic shallow-water vorticity equations, they should only apply in principle to the rotational momentum flux $\overline{u'_r v'_r}$ (we use r and d subscripts to refer to rotational and divergent anomalies, respectively, while overbars and primes denote zonal-mean values and deviations therefrom). Yet we showed in the companion paper (Zurita-Gotor 2019, hereafter Part I) that this rotational component only represents a small fraction of the observed tropical eddy momentum flux in the deep tropics. More fundamentally, Part I shows that the mechanism of eddy momentum convergence in the tropics is different from the extratropics, being associated with upper-level horizontal divergence over sectors with anomalous easterly zonal winds and upper-level horizontal convergence over sectors with anomalous westerlies, rather than with eddy vorticity fluxes. This pattern leads to an increase in the mass-weighted momentum and to an Eulerian acceleration in the presence of vertical (cross isentropic) momentum advection.

Tropical eddy momentum fluxes arise from spatial correlations between divergent eddy meridional velocities v'_d and rotational eddy zonal velocities u'_r: $\overline{u'_r v'_d}$. Part I refers to this correlation as the *divergent* eddy momentum flux, to distinguish it from the traditional rotational momentum flux $\overline{u'_r v'_r}$. This divergent eddy momentum flux is dominated by its stationary wave component, associated with zonal anomalies in the strength of the meridional overturning/Hadley cell and the climatological Rossby gyres. This decomposition of tropical eddy momentum transport requires some mechanism coupling the rotational and divergent anomalies. For instance, consider the relevant scenario of enhanced upper-level divergence over the warm pool in the summer hemisphere. In this scenario, we expect the cross-equatorial Hadley flow to be locally intensified over the same sector. However, whether this gives rise to northward or southward eddy momentum flux will depend on the sign of the rotational eddy zonal velocity, that is, on the phase of the rotational response to this divergent forcing. We argued in Part I that the answer to that question will depend on the closure of the vorticity balance.

This is the question that we aim to address with our study, which is organized as follows. Section 2 introduces the data and some definitions, and provides a quick overview of the main results in Part I. Section 3 uses a forced, homogeneous, linear model to predict the rotational response to divergent forcing, and shows that this model can reproduce quite well the observed, seasonally varying eddy momentum flux when it is forced by the observed divergent flow. Section 4 analyzes in some detail the dynamical determinants of the eddy momentum flux response in the simple model using the vorticity balance and section 5 investigates the relevance of that analysis in observations. We finish with some concluding remarks in section 6.

2. Data and conventions

We use in this paper the same ERA-Interim data (Dee et al. 2011) of Part I, which span the period 1979–2016. Data are defined on pressure levels at 2.5° resolution and the diagnostics presented in this paper represent an upper-troposphere average integrated over the 150–300-hPa layer. The horizontal velocities are decomposed into their rotational and divergent components (denoted with r and d subscripts, respectively), obtained by inversion of the vorticity and divergence fields. We also use monthly mean GPCP precipitation data (Adler et al. 2003) for some diagnostics.

Eddies are defined as differences from the zonal mean but we will focus in this paper on the *stationary* eddy momentum fluxes, which were shown to dominate the momentum transport in Part I. Because of the strong eddy momentum flux seasonality, however, this stationary circulation must be defined seasonally. We thus define a seasonal cycle of stationary eddy momentum transport computing for each calendar month the zonal mean of the products of the 37-yr monthly mean eddy velocity components. This procedure eliminates the submonthly and interannual variability but some of the slow intraseasonal variability may be contaminated into the seasonal cycle due to the limited record. However, Lee (1999) showed that the transient tropical eddy momentum flux is dominated by the interannual variability and Part I shows that the MJO contribution to the eddy momentum transport is an order of magnitude smaller than the stationary wave contribution.

Figure 1 shows the seasonal cycle of the rotational ($\overline{u'_r v'_r}$; black solid line) and divergent ($\overline{u'_r v'_d}$; black dashed line) contributions to the stationary cross-equatorial eddy momentum flux. The latter contribution dominates as noted in the introduction. Part I shows that this momentum flux reflects spatial correlations between the cross-equatorial Hadley flow v'_d and the rotational zonal velocity u'_r associated with the equatorial Rossby gyres. The change in sign of v'_d (the meridional overturning is always strongest over the warm pool region but its direction reverses following the shift of the heating to the summer hemisphere) as u'_r keeps a constant phase [easterly (westerly) eddy zonal winds are observed to the west (east) of the date line year-round] explains the observed seasonal reversal of the cross-equatorial eddy

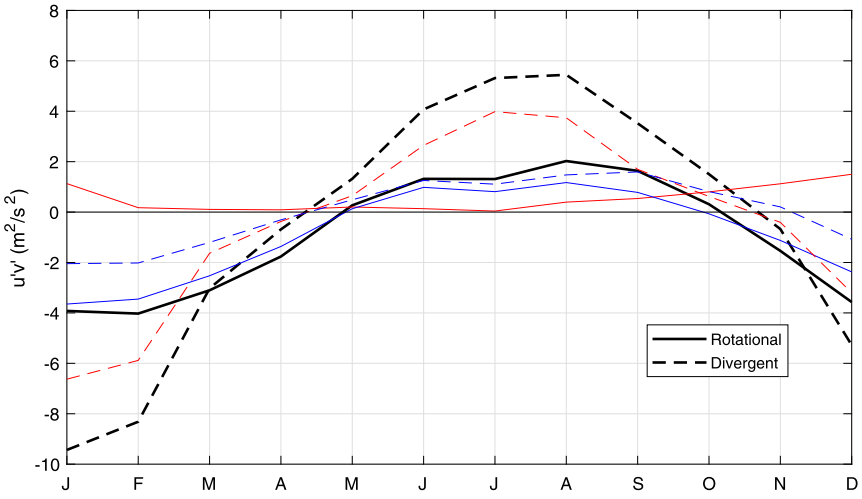

FIG. 1. Rotational (solid lines) and divergent (dashed lines) components of the stationary cross-equatorial eddy momentum flux. The black lines show the total flux, the red lines the $k = 1$ contributions and the blue lines the contributions by wavenumbers $k = 2$–3.

momentum transport. Part I also shows that the divergent momentum transport is dominated by the gravest zonal waves, especially $k = 1$ (red dashed line in Fig. 1). This large-scale time-mean pattern may reflect the aggregate effect of many individual convective events. Although the location of convection and cross-equatorial flow can be highly variable on day-to-day time scales (B. Hoskins 2018, personal communication), there is a clear preference for convection to occur west of the date line.

We will focus in this paper on the determination of the dominant $k = 1$ component of the stationary $\overline{u_r' v_d'}$ momentum flux. However, many of our conclusions also hold for other modes of momentum transport, stationary and transient, as illustrated in section 6 for the Madden–Julian oscillation (MJO). We study this phenomenon by regressing the dynamical fields on the MJO indices of Adames and Wallace (2014a; see Part I for more details).

3. A forced linear model

Consider the shallow-water vorticity equation on an equatorial beta plane:

$$\partial_t \xi + J(\psi, \xi + \beta y) - \nu \nabla^2 \xi = -(f + \xi) D - u_d \partial_x \xi - v_d (\beta + \partial_y \xi), \quad (1)$$

where ψ is the streamfunction for the rotational flow and $\xi = \nabla^2 \psi$ is relative vorticity. The last term on the left-hand side represents viscous damping and we split the horizontal advection term into its rotational and divergent components, included on the left- and right-hand sides of the above equation. This decomposition makes explicit the role of the divergent flow in forcing the vorticity equation through both vortex stretching and horizontal vorticity advection (Sardeshmukh and Hoskins 1988). In the following, we will refer to the left- and right-hand sides of this equation as the rotational tendency and divergent forcing, respectively.

Although the divergent forcing on the right-hand side of Eq. (1) also involves the rotational flow, this dependence disappears when the equation is linearized about a zonal basic state with horizontal velocities U and V:

$$\partial_t \xi' + U \partial_x \xi' + V \partial_y \xi' + \beta_e \partial_x \psi' - \nu \nabla^2 \xi' = -(f - \partial_y U) D' - v_d' \beta_e, \quad (2)$$

where $\beta_e = \beta - \partial_{yy} U$ is an equivalent beta and primed values denote perturbations.

As noted in the introduction, the mean meridional flow V plays an important role in theories of unforced propagation. We can see this by assuming plane-wave solutions of the form $e^{i(kx+ly-kct)}$, which leads to the following dispersion relation in the unforced and inviscid barotropic limit:

$$c = U + \frac{l}{k} V - \frac{\beta_e}{k^2 + l^2}. \quad (3)$$

With a slowly varying basic-state $U(y)$, $V(y)$, the above dispersion relation can be applied locally using a WKB approximation, implying Rossby wave refraction $l = f(y)$ as the basic state changes (Hoskins and Karoly 1981). For stationary waves, meridional propagation ($l^2 > 0$) requires $U + (l/k)V$ to be positive. As noted by Schneider and Watterson (1984) and Li et al. (2015), with

tropical easterlies propagation may still be possible when l has the same sign as V, which is associated with a meridional group velocity in the direction of V and an eddy momentum flux in the opposite direction. This is consistent with the observations showing an eddy momentum flux toward the wave-forcing region in the summer hemisphere through the tropical easterlies. Although this prediction strictly only applies to the rotational eddy momentum flux $\overline{u_r'v_r'}$, we show in appendix A that when the necessary condition for propagation is satisfied the divergent momentum flux reinforces the rotational momentum flux, becoming the dominant term in the long-wave limit.

However, a theory of unforced propagation is unlikely to explain the observed tropical momentum fluxes in the strongly convecting terrestrial atmosphere. As discussed in Part I, the divergent momentum fluxes are associated with a region of strong momentum convergence/eddy generation adjacent to the equator in the summer hemisphere (see Figs. 7b and 8b in Part I), pointing to the important role of the forcing for the determination of these fluxes. Motivated by this, we study the *forced* $\overline{u_r'v_d'}$ response to tropical heating assuming that this heating is determined independently of the circulation as in classical tropical circulation theory (e.g., Gill 1980). Under a weak temperature gradient approximation $D' \approx Q'$, prescribing the heating is equivalent to prescribing the full divergent field. We thus use the observed D' and v_d' to force the vorticity equation [Eq. (2)] and calculate the divergent eddy momentum flux $u_r'v_d'$ using the rotational wind response u_r' to this divergent forcing.

As will be shown in the next section, the closure of the vorticity balance can be very different for eddies of different meridional scales. Our focus in this paper will be on the gravest meridional modes, which we will show to dominate the momentum transport. Aiming to uncouple the meridional modes, we use a homogeneous formulation with constant U, V, and β_e, under the assumption that the meridional structure of the forcing determines to first order the structure of the forced response, with little role for the basic state (this is a poor approximation in the subtropics, where vorticity shearing is important). For the same reason, we use a plane formulation in the meridional domain $\phi \in [-\pi/2, \pi/2]$. The results are very similar using a spherical harmonics expansion (not shown) but the meridional modes are formally coupled through the Laplacian in that case.

With these assumptions, Eq. (2) becomes for a stationary mode with wavenumbers k and l:

$$-(ikU + ilV)(k^2 + l^2)\hat{\psi} + ik\beta_e\hat{\psi} - \nu(k^2 + l^2)^2\hat{\psi} = -\widehat{fD} - \beta_e\hat{v}_d, \quad (4)$$

using circumflex accents to denote spectral space variables (note in particular that $\widehat{fD}$ is the Fourier transform of the full fD' product).

We solve Eq. (4) for the dominant zonal wavenumber $k = 1$ as follows. For each calendar month, we define U and V as the climatological zonal-mean zonal and meridional winds averaged over the equatorial band $|\phi| \le 10°$ and calculate an effective β_e that also incorporates the relative vorticity gradient (averaged over the same band). To isolate the tropical forcing, we multiply the climatological monthly mean $-fD' - v_d'\beta_e$ by a meridional Gaussian with half-width 40° before computing its meridional Fourier transform. Using Eq. (4), we calculate the rotational response $\hat{\psi}$ and $\widehat{u_r} = -il\hat{\psi}$ for each harmonic of the forcing, and then the divergent momentum flux $\overline{u_r'v_d'}(k = 1, y)$ using the observed v_d' and the predicted u_r' (converted back to physical space).

Use of an effective beta improves the quantitative agreement with observations by increasing the amplitude of the response but the results are not very sensitive to the other modeling choices. In contrast, the results are fairly sensitive to the viscosity coefficient ν, chosen to damp the resonant wavenumber ($|l_0| \approx 4$) with a time scale of 1.5 days. The results are similar for moderate variations (doubling or halving) in this parameter but when much longer time scales are used the solution becomes dominated by the resonant mode, while for shorter time scales there is a significant amplitude loss. Our use of the more scale-selective viscous damping (as opposed to linear vorticity damping) is motivated by the weak scale separation between the resonant mode and the scales that dominate the momentum transport (as shown below).

This procedure produces the $u_r'v_d'$ seasonal cycle in Fig. 2b, which should be compared to the observed $k = 1$ stationary seasonal cycle in Fig. 2a. The predicted momentum flux is a bit too weak (note the different color scale in both panels), particularly during DJF, and some differences are also apparent near the winter subtropics, where the large zonal wind and significant wind shear would be expected to play a role in the vorticity balance (Monteiro et al. 2014; Kraucunas and Hartmann 2007). Nevertheless, the skill of the model in capturing the observed seasonal cycle is striking given the crudeness of the approximations involved. In contrast, the rotational momentum flux is not well reproduced by the model (not shown), which is not surprising in the absence of extratropical forcing.

To investigate the relative importance of vortex stretching and meridional divergent advection for the model's response, we have repeated the analysis forcing the model with each of the terms on the right-hand side of Eq. (4) in isolation. Figures 2c and 2d show that

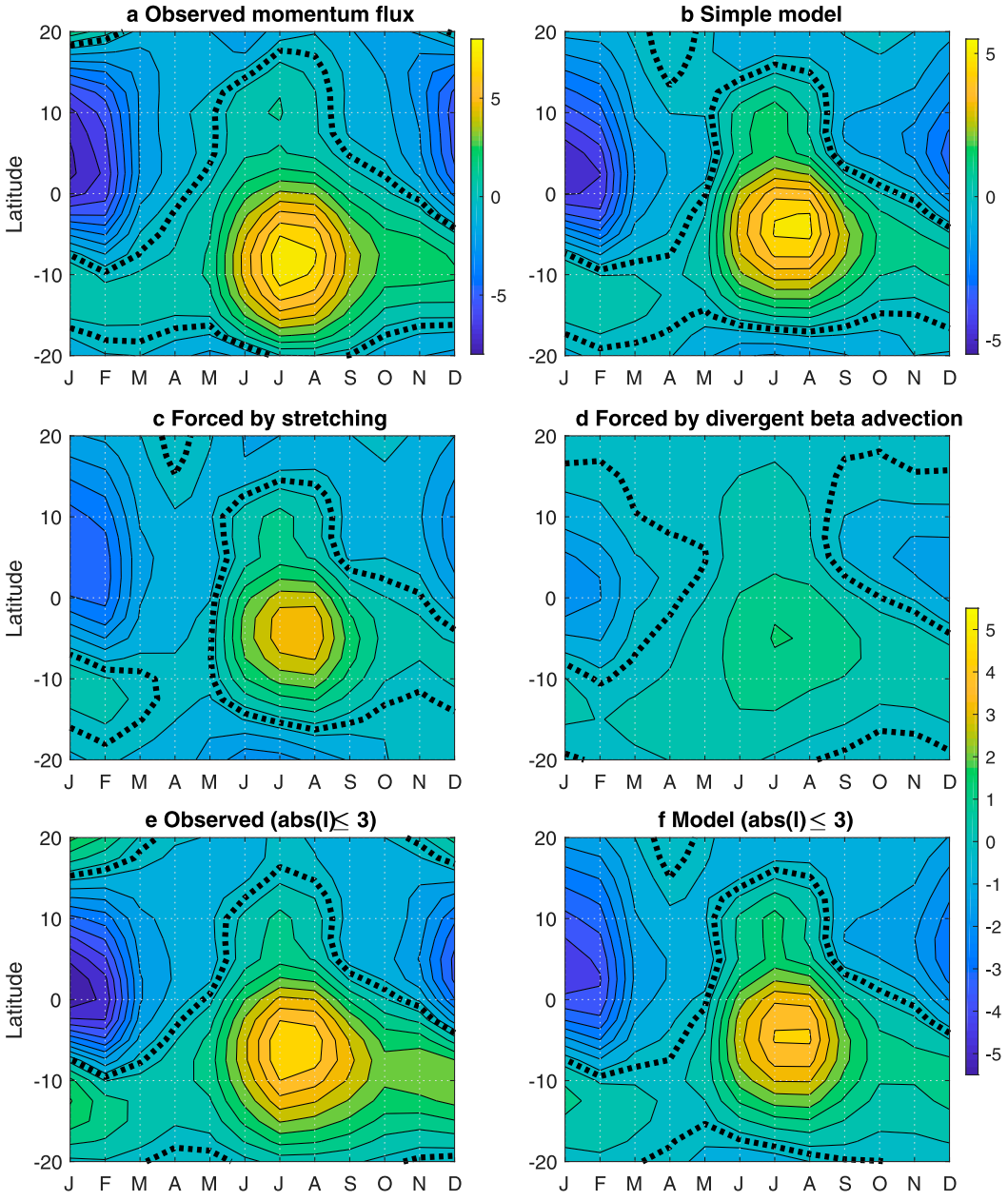

FIG. 2. Seasonal cycle of $k = 1$ stationary eddy momentum flux $\overline{u_r' v_d'}$ ($m^2 s^{-2}$): (a) observed, (b) prediction by the simple model, (c) model's response to vortex stretching, and (d) model's response to divergent beta advection. (e),(f) As (a) and (b), but computing the fluxes using only modes with $|l| \leq 3$ in observations and model, respectively. Note the use of a different color scale in (a) versus all other panels.

the two forcings produce a response of the same sign (a momentum flux from the winter to the summer hemisphere) but the model's response to stretching is significantly larger. Section 4b discusses in more detail the dynamics of the two responses.

Likewise, we can investigate the role played by changes in the eddy forcing and in the basic state for the seasonal cycle of the eddy momentum flux in our model. The left panels of Fig. 3 show that the mean tropical winds play virtually no role for the determination of the eddy momentum flux, as the results when fixing U and V to their climatological DJF or JJA values and when using zero winds are very similar to those with seasonally dependent winds. This implies that the seasonal dependence of the eddy momentum flux in the model must be due to seasonal changes in the eddy forcing, as indeed confirmed by the right panels of Fig. 3. We provide an interpretation of these results in the next section.

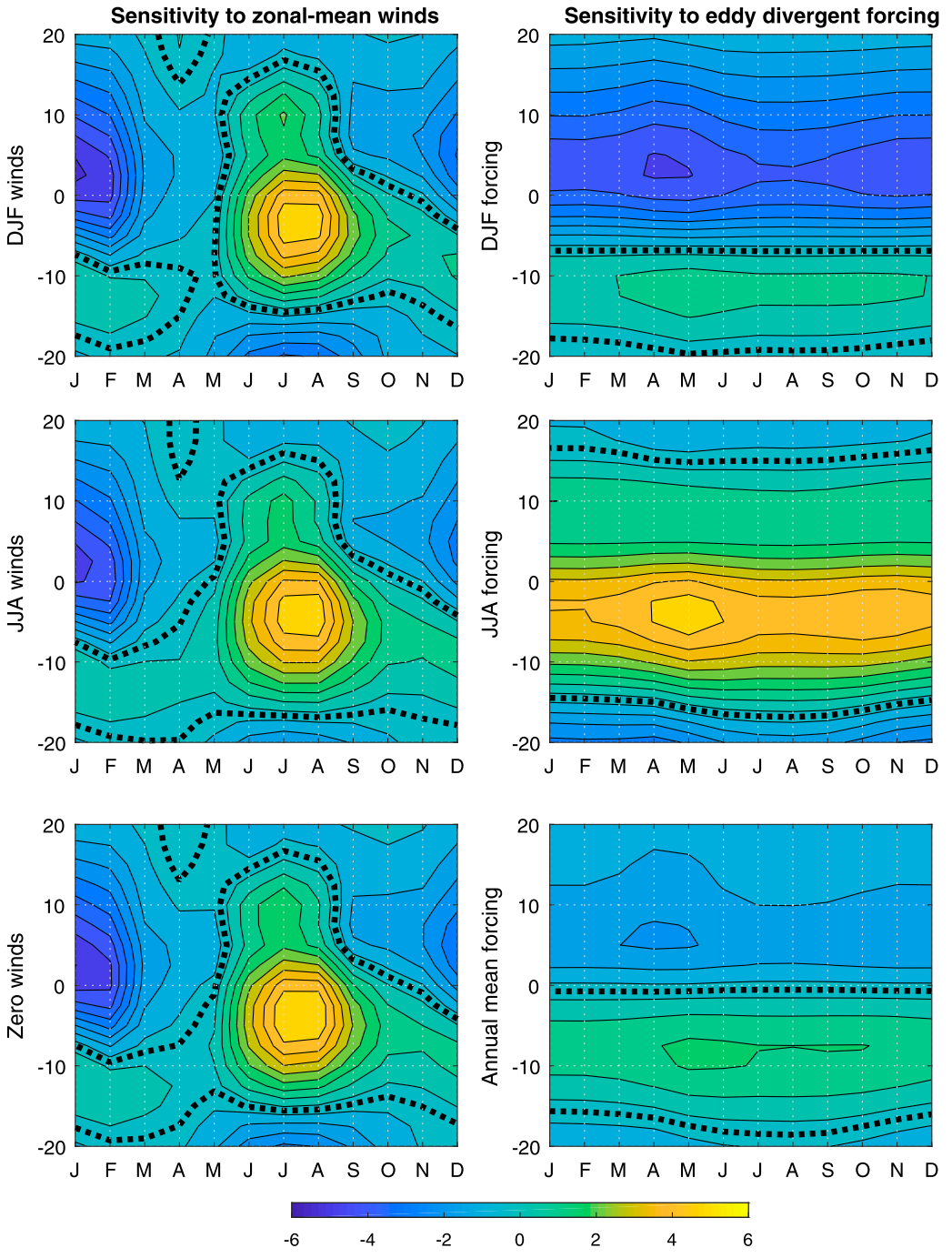

FIG. 3. (left) Model's sensitivity to prescribed mean winds U and V: (top) climatological DJF winds, (middle) climatological JJA winds, and (bottom) $U = V = 0$. (right) Model's sensitivity to prescribed divergent forcing: (top) DJF divergence, (middle) JJA divergence, and (bottom) annual-mean divergence. All panels show the stationary divergent momentum flux $\overline{u_r' v_d'}$ ($\mathrm{m^2\,s^{-2}}$).

4. Dynamical analysis

a. *Natural frequency and dominant meridional scales*

The rotational response in our model is constrained by the requirement that the vorticity tendency balances the prescribed vorticity forcing by the divergent field. To analyze the determinants of the seasonal cycle, it is useful to rewrite Eq. (4) in the form

$$-i(k^2 + l^2)\omega_0 \hat{\psi} = \hat{F}, \tag{5}$$

where

$$\omega_0(k,l) = kU + lV - \frac{\beta_e k}{k^2 + l^2} \tag{6}$$

is the natural frequency for wavenumbers k and l implied by the dispersion relation (ignoring the imaginary component of ω_0 due to damping). In our linear model, the sensitivity of the solution to the mean flow U and V is manifested through this term.

As discussed in section 3, the asymmetry in Rossby's dispersion relation due to the meridional Hadley flow V plays an important role in theories of (unforced) Rossby wave propagation in the tropics (Li et al. 2015). A related argument is that with easterly or weak westerly U, modes with $Vl > 0$ have a smaller $|\omega_0|$ and hence a stronger response to forcing. In particular, the propagating wavenumber l_0 predicted by the unforced theory $\omega_0(k, l_0) = 0$ is resonant in the forced problem. For forcing of this scale, the amplitude of the response is only constrained by damping in our model. The impact of resonance is emphasized by the study of Arnold et al. (2012), who find abrupt transitions in the circulation of an idealized model due to the resonant amplification of the tropical eddy momentum flux when the basic state changes. Beyond resonance, the meridional-scale l_0 is associated with a change in the sign of the response. With $Vl < 0$, or with $Vl > 0$ and $|l| < |l_0|$, the sign of ω_0 agrees with that of the beta term and the streamfunction minimum (vorticity maximum) is found a quarter wavelength to the west of the positive vorticity forcing. The opposite is true when $Vl > 0$ and $|l| > |l_0|$, in which case the vorticity maximum is found a quarter wavelength to the east of the vorticity forcing.

Figure 4 shows the structure of $\omega_0(k, l)$ for $k = 1$ and DJF (blue) or JJA (red) basic states, normalized by the beta contribution $-\beta k/(k^2 + l^2)$. As expected, the resonant wavenumber l_0 changes sign between both seasons, as it must satisfy $Vl_0 > 0$. In contrast, its scale is very similar during DJF and JJA ($|l_0| \approx 4$) because ω_0 is insensitive to U for this small value of k, and V essentially reverses between seasons. The response of the model to forcings with meridional-scale $|l_0|$ is evidently sensitive to V, and Fig. 4 shows that the same is true for shorter waves. However, for $|l| \leq 3$ the natural frequency is only weakly sensitive to l and is well approximated by the β term (dashed lines). These are the scales that dominate the model's response because the large model viscosity, chosen to damp the resonant-scale $|l_0| = 4$ with a time scale of 1.5 days, strongly damps wavenumbers at scales $|l| \geq |l_0|$. (The black line in Fig. 4 shows the imaginary component of ω_0 as a function of wavenumber).

The model's success suggests that these large meridional scales are also primarily responsible for the observed momentum transport. To assess the scales of

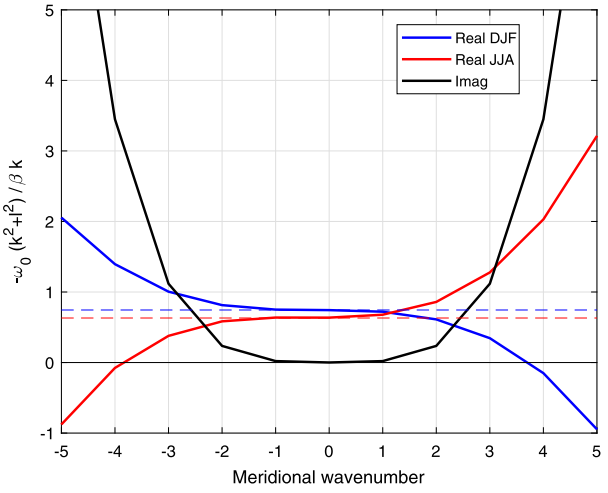

FIG. 4. Natural frequency ω_0 for $k = 1$ as a function of meridional wavenumber, normalized by the beta contribution $-\beta k(k^2 + l^2)^{-1}$. The blue and red lines show, respectively, the real DJF and JJA components using the observed winds (solid) and $U = V = 0$ (dashed; note that we still use an equivalent β). The black line shows the imaginary component due to damping.

dominant momentum transport in model and observations, we have decomposed the meridionally averaged momentum flux between 20°S and 20°N (shown in Fig. 5a) into contributions by different meridional wavenumbers. This metric is a sensible measure of the tropical momentum flux, as the momentum flux is nearly one signed during both solstice seasons (cf. Fig. 2). To compute the contributions of each meridional wavenumber to this metric, we expand u'_r into its meridional Fourier components and calculate their individual contributions to the integrated $u'_r v'_d$ using the *full* v'_d. Note that because the meridional modes are only orthogonal when integrated over the full sphere rather than between −20° and +20°, this also includes mixed wavenumber contributions $\widehat{u_r}(l)\widehat{v_d}(l')$ with $l \neq l'$. Although these mixed contributions are relatively small, they are not strictly zero—this is why we refer to this diagnostic as the "pseudocospectrum." We did not compute the actual cospectrum for the integrated momentum flux between 90°S and 90°N because that metric is sensitive to the high-latitude structure.

Figure 5b shows that the observed momentum flux is dominated by long waves, especially during JJA. During DJF, shorter-scale contributions to the eddy momentum flux are found around $l = -4$ (this is *not* due to resonance as $l_0 = +4$ during this season). This component of the response is strongly damped in our model, which predicts the peak flux at longer meridional scales (Fig. 5c). More generally, the largest differences between the observed and modeled pseudocospectra are found at $|l| \geq 3$. This suggests that the low eddy

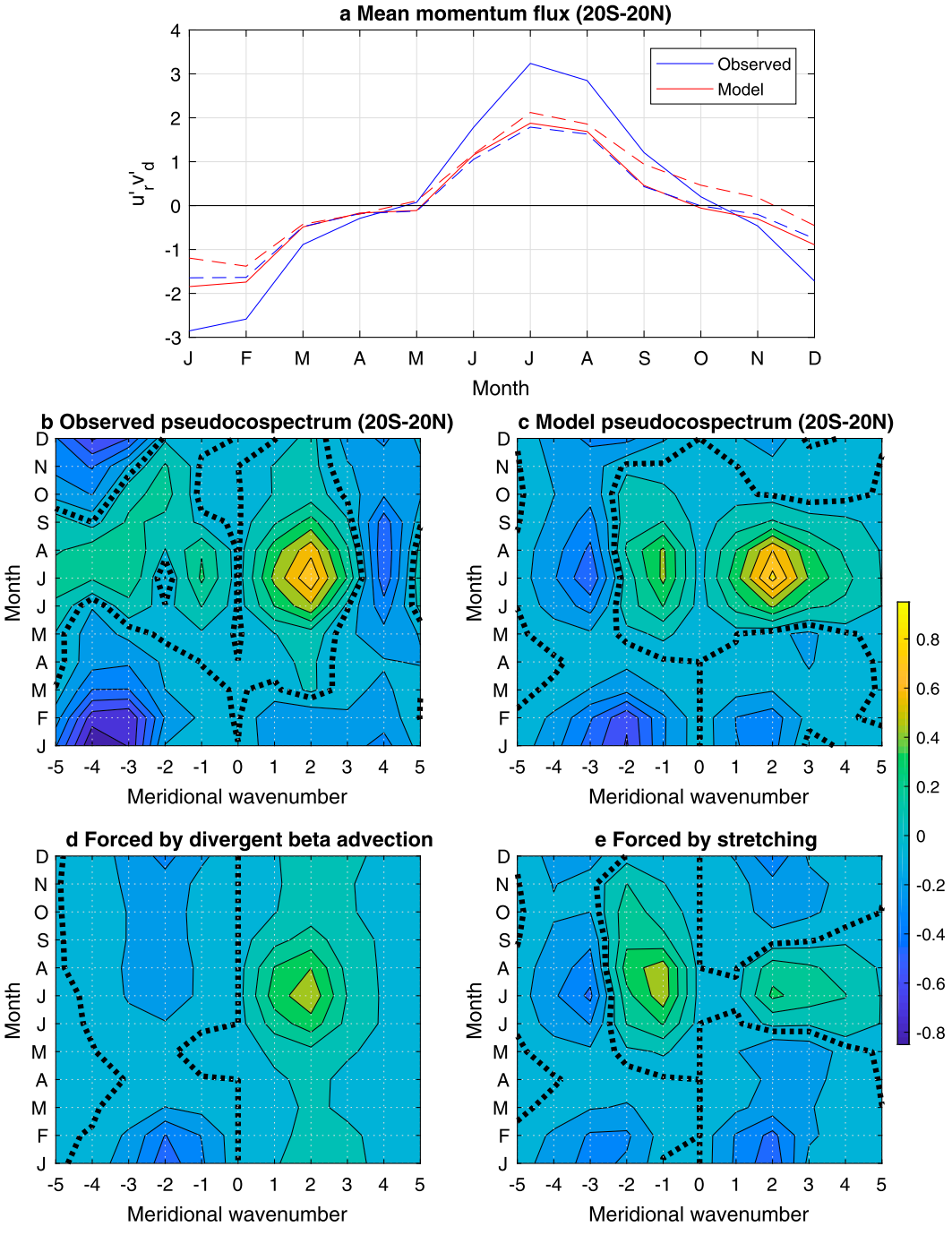

FIG. 5. (a) Eddy momentum flux, integrated between 20°S and 20°N in observations (blue) and the model (red). The dashed lines show the mean flux computed using only modes with $|l| \leq 3$. (b) Meridional pseudocospectrum (see text for details) of the mean 20°S–20°N eddy momentum flux in observations. (c) As in (b), but for the model. (d),(e) As in (c), but when the model is only forced by divergent beta advection and vortex stretching, respectively.

momentum flux bias in the model might be partly due to the strong damping of scales shorter than $|l| = 3$. This hypothesis is supported by Fig. 5a (dashed lines), which shows that the seasonal cycle of the mean eddy momentum flux between 20°S and 20°N is very similar in observations and model when only contributions by modes with $|l| \leq 3$ are included. The impact of modes with $|l| > 3$ can be further appreciated by comparing Figs. 2e and 2f (computed including only modes with $|l| \leq 3$) with Figs. 2a and 2b. Eliminating the contribution

by modes with $|l|>3$ to the observed eddy momentum flux leads to a significant reduction in this flux, so that the model's response (which is not as affected) is in better quantitative agreement.

b. Divergent forcing and momentum flux direction

As noted in Part I, while the sign of the rotational momentum flux is determined by the tilt of the streamlines, the sign of the divergent momentum flux depends instead on the phase relation between the rotational and the divergent flow. When the rotational flow is simply forced by the divergent flow as assumed in this section, this phase relation is determined by the closure of the vorticity balance. In this section, we investigate what aspects of the divergent eddy forcing and the mean state determine the direction of the divergent momentum flux.

This is trivial to assess for the part of the flow forced by meridional divergent advection. Substituting $\hat{F}=-\beta_e\hat{v_d}$ in Eq. (5) with $\hat{u_r}=-il\hat{\psi}$, we obtain

$$\overline{u_r'v_d'}^{\beta}=-\frac{\beta_e l|\hat{v_d}|^2}{2(k^2+l^2)\omega_0}. \tag{7}$$

The direction of the momentum flux depends on the sign of $\omega_0 l$. For the long waves shown to dominate the pseudocospectrum, $\omega_0<0$ and the sign of $\overline{u_r'v_d'}$ agrees with that of l. The direction of $\overline{u_r'v_d'}$ is still determined by the tilt of the phase lines, but *its sign is opposite to that of the rotational momentum flux*. Figure 6a illustrates the structure of this solution for $l<0$. With $\omega_0<0$ the sign of the vorticity tendency is determined by β, so the rotational flow must point northward to the east of the divergence maximum to balance the positive vorticity forcing by $-\beta_e v_d'$ at the filled red circle. With $l<0$, $\psi'<0$ ($\psi'>0$) over the region of upper-level divergence (convergence) and ψ' and χ' are in phase. The contrary occurs for $l>0$ (Fig. 6b), in which case the rotational flow points southward to the east of the divergence maximum and ψ' and χ' are 180° out of phase. In both cases, the streamfunction minimum (vorticity maximum) is found a quarter wavelength to the west of the positive vorticity forcing (indicated with a filled red circle) because $\omega_0<0$. The contrary would be observed for shorter waves with $\omega_0>0$.

The configuration in Fig. 6a (Fig. 6b) is associated with a southward (northward) divergent momentum flux $\overline{u_r'v_d'}$, which opposes the northward (southward) momentum flux by the rotational flow $\overline{u_r'v_r'}$. In the limit in which the vorticity tendency is dominated by β, the rotational and divergent fluxes compensate exactly as Eq. (4) then reduces to a balance between rotational and divergent beta advection: $v_r'=-v_d'$. This corresponds to the simple thought example discussed in Part I (in that example $\overline{u_r'v_r'}$ and $\overline{u_r'v_d'}$ vanish because there is no phase tilt). More generally, when the mean flow advection is not negligible $\overline{u_r'v_d'}$ will dominate when $|\omega_0|>\beta_e k/(k^2+l^2)$. Figure 5d shows that the $\overline{u_r'v_d'}$ pseudocospectrum produced by the model when it is only forced by $-\beta_e v_d'$ agrees qualitatively with these predictions: modes with positive (negative) l are associated with northward (southward) eddy momentum transport. The former (latter) are dominant during JJA (DJF), so that $Vl<0$ during both solstice seasons (implying no role for resonance).

We next discuss the $\overline{u_r'v_d'}$ response to vortex-stretching $F'=-fD'$, which dominates the full response in our model. Consider first the case in which the Coriolis parameter is constant: $f=f_0$ (Fig. 6c). With positive f_0, vortex stretching produces a negative vorticity forcing over the divergence maximum, which must be balanced by vorticity advection by southward rotational flow (assuming again that $\omega_0<0$). As shown in Fig. 6c, this produces a streamfunction response in quadrature with the divergence anomaly so that there is no divergent momentum flux: $\overline{u_r'v_d'}=0$.

It is thus key to take into account the meridional f structure to obtain a nonzero momentum flux response. Figure 6d shows the response to the forcing $-(f-f_0)D'$ (where f_0 is the mean Coriolis parameter over the scale of the wave)[1] using the same divergence field as in Fig. 6c. Northward of the latitude where $f=f_0$ there is again negative vorticity forcing and southward rotational flow, but southward of that latitude the vorticity forcing is positive and the rotational flow northward. The rotational circulation must then be closed by a component perpendicular to the divergence phase lines (note that the D' and ψ' phase lines can no longer be aligned), in the direction of v_d'. As shown in Fig. 6d this produces a southward momentum flux when l is negative, while the contrary is true when l is positive (Fig. 6e). This is consistent with our findings that the model responses to vortex stretching and divergent advection have the same sign (cf. Figs. 2c and 2d).

With nonconstant f, it is not possible to find a simple expression for the momentum flux similar to Eq. (7). A divergent mode with meridional wavenumber l does not force a rotational flow of the same scale and the pseudocospectrum has a complicated structure (Fig. 5e). The analysis is simplified if we can assume that the vorticity tendency is dominated by β (or more generally, if we can neglect meridional derivatives). In that limit, it is shown in appendix B that for a slowly varying

[1] The fact that the divergent momentum flux is sensitive to the range of variability of f, rather than to its mean value, is key to the impact of vortex stretching for the model's response in spite of the small values of f near the equator. These arguments also suggest that the impact of vortex stretching will be larger for waves of longer meridional scales.

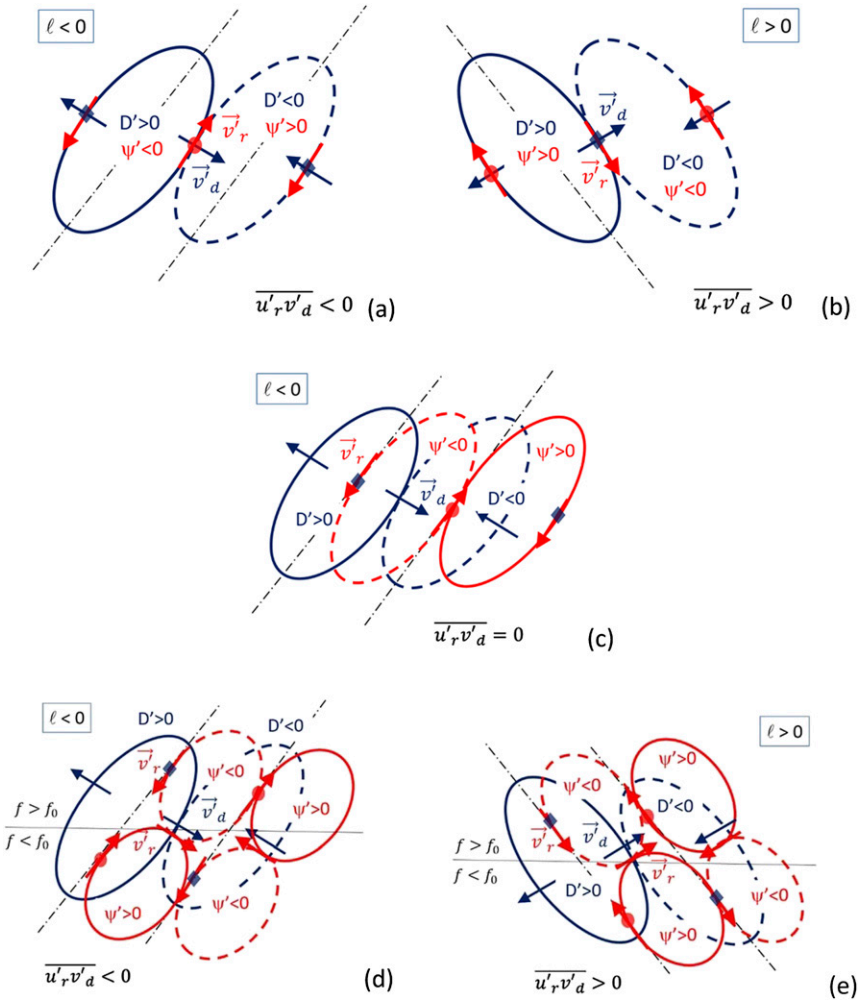

FIG. 6. Sketch illustrating the rotational circulation forced by prescribed divergent forcing and the associated momentum flux $\overline{u'_r v'_d}$ when $\omega_0 < 0$. (a) Response to $-\beta v'_d$ with $l < 0$. (b) As in (a), but with $l > 0$. (c) Response to $-f_0 D'$ with constant f_0. (d) Response to $-(f - f_0)D'$ with $l < 0$. (e) As in (d), but with $l > 0$. In all panels, we indicate the maximum positive (negative) forcing with a filled red circle (blue diamond). The divergent velocity vector $\mathbf{v}'_d$ (blue) is drawn pointing from the divergence maximum to the divergence minimum, while the rotational velocity vector $\mathbf{v}'_r$ (red) is inferred assuming that the vorticity tendency $\sim v'_r \beta$ balances the vorticity forcing. With $\omega_0 < 0$, the streamfunction minimum is located one-quarter wavelength to the west of the positive vorticity forcing. The direction of $\overline{u'_l v'_d}$ is inferred from the sign of the zonal component of $\mathbf{v}'_r$ and the meridional component of $\mathbf{v}'_d$. Note that the phase slope is exaggerated for clarity because $k \ll l$.

divergence field the response to vortex stretching approaches the response to divergent meridional advection (and is thus determined by the tilt of the divergence phase lines). However, the two responses can differ significantly when the divergence field has meridional structure.

5. Closure of the vorticity balance and divergence phase tilt in observations

Although the simple arguments presented in the previous section can help explain the sensitivity of the idealized model, their actual relevance for the observed momentum flux is a bit more questionable given the crude assumptions of the simple model. In particular, our arguments rely heavily on (a very simplified version of) the vorticity balance that may not be appropriate for observations. The closure of the observed tropical vorticity balance is subject to big errors even in modern reanalysis products (e.g., Yang and Hoskins 2017), as it has been known for a long time that transience and nonlinearity play an important role for this balance (Sardeshmukh and Hoskins 1985).

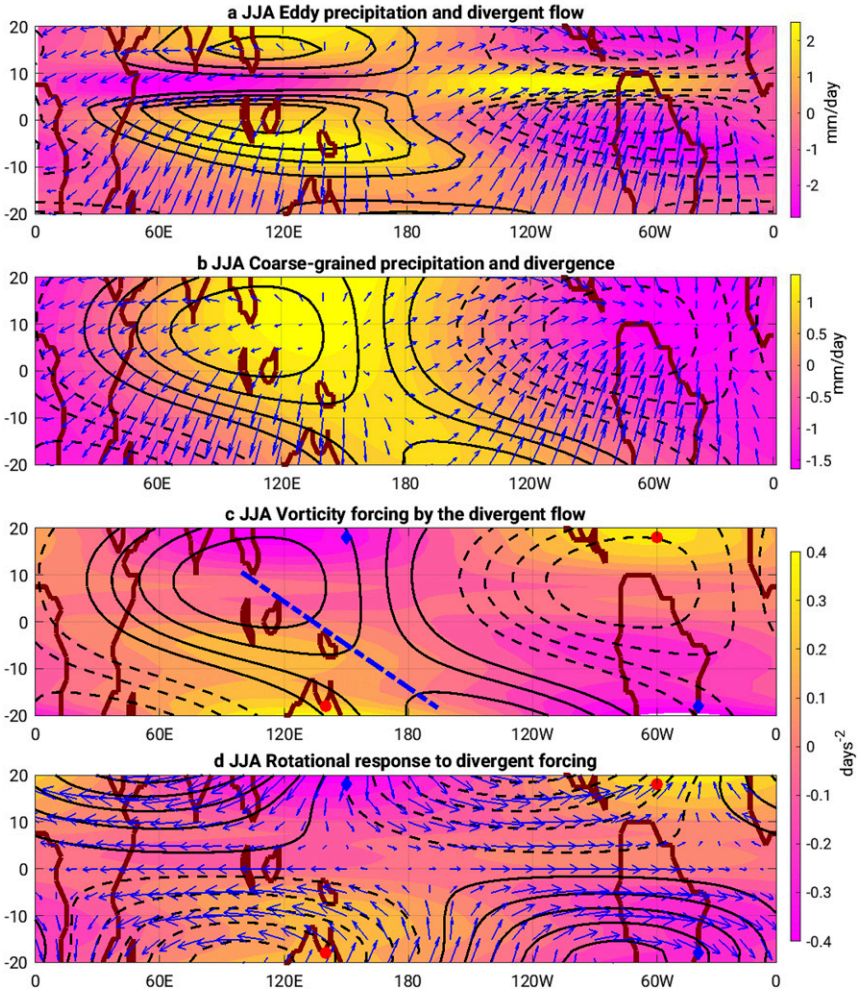

FIG. 7. JJA climatology of $k = 1$ (a) eddy precipitation (color shading), eddy upper-level divergence (contours), and eddy divergent velocity (blue vectors); (b) coarse-grained ($|l| \leq 3$) precipitation and divergence as in (a); (c) coarse-grained divergence (contours; the thick axis line emphasizes the phase tilt) and the vorticity forcing by the divergent flow (color shading; we emphasize the positive and negative extrema using filled red circles and blue diamonds, respectively); and (d) eddy rotational streamfunction (contours), rotational vorticity tendency [color shading, with markers as in (c)], and eddy rotational velocity (blue vectors).

We contend that the aforementioned difficulties in closing the tropical vorticity balance are mainly due to the small scales, those most affected by nonlinearity, while the large scales found to dominate the meridional eddy momentum transport can be reasonably understood using the idealized vorticity closure equation, Eq. (4). In support of this argument, we show below that the simple relations between the divergent forcing and the rotational response that constrain the sensitivity of the eddy momentum flux in the model are also at work for the observed JJA and DJF flows.

Focusing on JJA first, Fig. 7a shows the $k = 1$ eddy precipitation field (shading), upper-level (150–300-hPa average) divergence (contours), and upper-level divergent wind vectors. Although the divergent wind is evidently related to the precipitation and divergence fields, it is also apparent that the latter have finer spatial structure than the winds, as expected for a differenced field. This is consistent with our findings that the eddy momentum flux is primarily determined by the gravest meridional modes of the divergence field. As shown in Fig. 7b, the coarse-grained ($|l| \leq 3$) precipitation and divergence fields capture the gross structure of the divergent wind, its direction being determined by the mean phase tilt as in the sketches of Fig. 6.

The shading in Fig. 7c shows the net vorticity forcing by the (nonfiltered) divergence field. We emphasize with filled red circles (blue diamonds) in this figure the

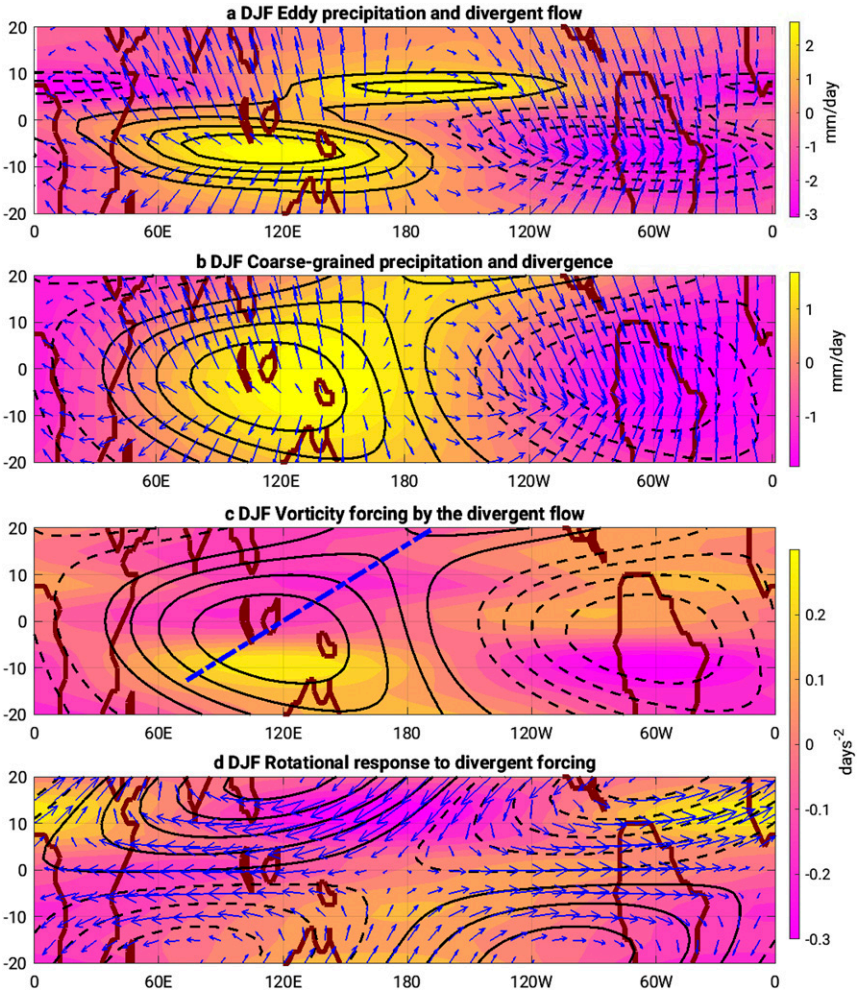

FIG. 8. As in Fig. 7, but for DJF.

approximate locations of maximum positive (negative) vorticity forcing in both hemispheres. For a divergence field with $l > 0$ as observed, we expect to find the maximum divergent-advection forcing near the western node of the divergence (cf. Fig. 6b), and the maximum vortex-stretching forcing near the axis of maximum convergence (divergence) at some distance from the equator in the Northern (Southern) Hemisphere (cf. Fig. 6e). The observed maxima lie somewhere between these two limits, though vortex stretching appears to be more important in the Northern Hemisphere and divergent advection appears to be more important in the Southern Hemisphere.

On the other hand, the shading in Fig. 7d shows the rotational tendency, linearized about the time- and zonal-mean flow as on the left-hand side of Eq. (2) [note that we took into account the meridional structure of the basic-state $\overline{u}(y)$, $\overline{v}(y)$ to compute the mean-flow advection for increased accuracy]. It is apparent that even in this simplified form, the rotational tendency balances quite well the observed divergent forcing, the small phase bias likely due to the neglect of nonlinear zonal eddy advection. Consistent with $\omega_0 < 0$ for the dominant grave meridional waves, we observe northward (southward) rotational flow over regions with positive (negative) vorticity forcing, so that the streamfunction minimum is found to the west of the positive vorticity forcing as expected. Because the vorticity forcing is roughly antisymmetric about the equator (Fig. 7c), the streamfunction field has a quadripolar structure. Finally, we note that the northward eddy momentum flux observed during this season (cf. Fig. 2) is consistent with the northwest-to-southeast tilt ($l > 0$) of the divergence phase lines based on the arguments of the previous section.

Figure 8 shows a similar analysis during DJF. The negative eddy momentum flux during this season is consistent with the northeast-to-southwest tilt ($l < 0$) of the coarse-grained divergence. The balance between divergent forcing and rotational tendency is, however,

significantly worse than before, suggesting that other terms may be important for the vorticity balance as also found for this season by Sardeshmukh and Hoskins (1985). Since the meridional pseudocospectrum peaks at smaller scales during this season,[2] we expect nonlinearity to play a bigger role than during JJA. Additionally, the vorticity fluxes by eddies of extratropical origin are likely more important during DJF than during JJA because the summer extratropical hemisphere is more active during DJF and extratropical eddies forced in the winter hemisphere are also able to penetrate deeper into the tropics during this season (Zurita-Gotor and Álvarez-Zapatero 2018). In this regard, it is noteworthy that the streamfunction field in Fig. 8d has a pronounced northeast-to-southwest tilt, in contrast with the nearly standing pattern in Fig. 7d. Such a tilt is associated with northward rotational eddy momentum fluxes during this season by zonal wave $k = 1$ (see Fig. 1), opposite to the divergent momentum fluxes, and with Rossby wave propagation from the winter to the summer hemisphere. The simple model is unable to reproduce this behavior, though it is unclear if this is due to a deficiency of the model or to the lack of extratropical forcing. While all these factors may contribute to the poor closure of the vorticity balance during DJF, the model still appears to be relevant for explaining the divergent momentum flux during this season.

6. Concluding remarks

In this paper we have analyzed the mechanisms coupling the divergent and rotational circulations aiming to understand the determination of the observed tropical eddy momentum flux, associated with correlations between the divergent eddy meridional velocity and the rotational eddy zonal velocity. We showed that a simple homogeneous, linear model with uniform basic-state winds can reproduce quite well the observed momentum flux when the rotational circulation is forced by the observed divergent flow, which suggests that the eddy momentum flux can be understood as a response to the divergent forcing. We found our simple model to display very little sensitivity to changes in the mean state, in contrast to previous studies showing significant eddy momentum flux modulation by the Hadley cell (Kraucunas and Hartmann 2007). In the context of a forced linear model, the sensitivity to the basic state is associated with changes in the natural frequency of the system and a possible transition to resonance of the sort described by Arnold et al. (2012). The inevitable nonlinearity near the resonant scale cannot be resolved by our simple model, which uses strong scale-sensitive damping to prevent resonant behavior. We would expect more sensitivity of the solution to the basic-state winds in a nonlinear model that can resolve these and shorter scales.

As changes in the basic state have little bearing on the determination of the eddy momentum flux, the single most important factor affecting the seasonal reversal of the momentum flux in our model is the seasonal variability in the divergent forcing. We found that vortex stretching and divergent beta advection produce responses with the same sign—a momentum flux directed from the winter to the summer hemisphere—but the former is about twice as large. We can understand these responses by noting that for the long waves that dominate the momentum transport the natural frequency ω_0 is negative and the vorticity maximum is shifted a quarter wavelength to the west of the positive vorticity forcing (indicated with a filled red circle in all the sketches of Fig. 6). We showed that with both types of forcing the eddy momentum flux response is positive (negative) when the divergence anomalies have a northwest-to-southeast (northeast-to-southwest) tilt, which is consistent with observations. Note that this is opposite to the classical relation between rotational eddy momentum flux and streamfunction phase tilt, so that we expect the divergence and streamfunction contours to tilt in opposite ways when the rotational and divergent momentum fluxes have the same sign. Reversibly, when the divergence and streamfunction contours have the same tilt the rotational and divergent momentum fluxes tend to cancel each other, as found for instance for $k = 1$ during DJF (cf. Fig. 8).

The important role played by the divergence phase tilt underscores a crucial limitation of our analysis: the use of a prescribed divergence field. It is now well recognized that the heating is not independent of the circulation in the tropics. Our results provide an eloquent validation to this axiom: even though the mean heating is thought to be mainly determined by the boundary conditions (Hoskins et al. 1999), we cannot think of any obvious reason why the divergence field should tilt in opposite meridional directions during both solstice seasons. It seems more likely that the seasonal reversal of the phase tilt in observations should be associated with changes in meridional wave propagation as the wave source moves into the summer hemisphere (Dima et al. 2005). Because Rossby waves have westerly pseudomomentum, they transport easterly momentum as they propagate and converge momentum into their source region. In the extratropics the eddy momentum flux is dominated by the rotational flow, so the streamfunction field must tilt westward with latitude away from the

[2] Note that only the divergence field is coarse grained in Figs. 7 and 8, but not the vorticity forcing or the rotational response. The filtered fields are in better agreement (not shown).

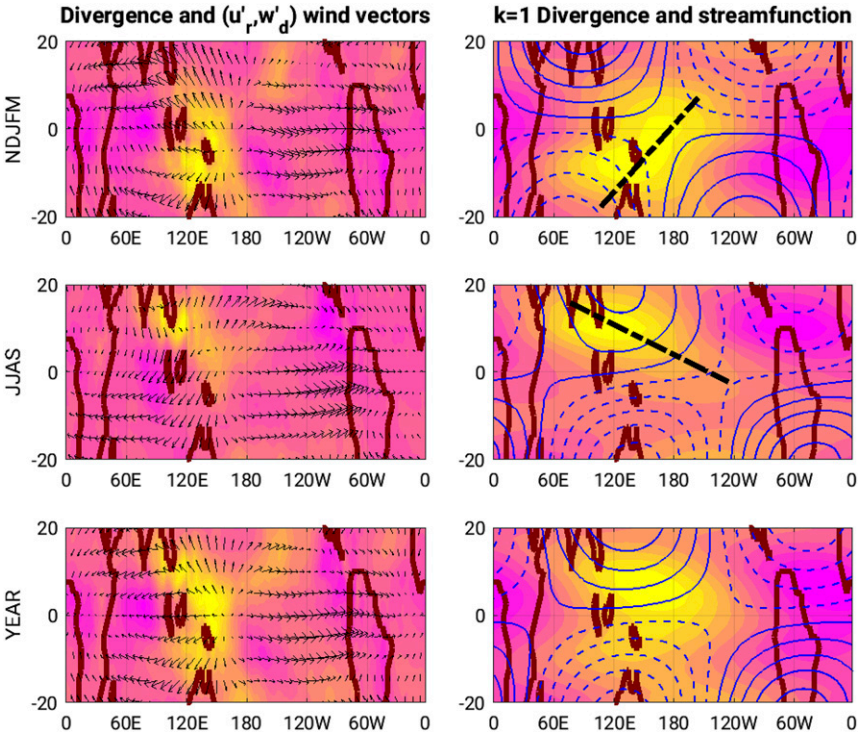

FIG. 9. (top) NDJFM, (middle) JJAS, and (bottom) full-year MJO regressions of (left) upper-level divergence and (u_r', v_d') wind vectors and (right) gravest ($k = 1$) zonal component of the divergence (color shading; the thick axis line emphasizes the phase tilt) and streamfunction fields (contours). For all seasons, the regressions shown correspond to the MJO phase with maximum velocity potential difference at 150°E.

source region to produce eddy momentum convergence into that latitude. Along similar lines, we speculate that the observed eastward phase tilt of the divergence field moving from the summer hemisphere to the winter hemisphere is linked to the requirement that the divergent momentum flux, dominant in the tropics, converges momentum into the source region. As Figs. 7b and 8b show, this phase tilt has important implications for the large-scale distribution of precipitation in the tropics.

Under this perspective, what we have described here as a forced rotational response could perhaps be better regarded as coupled rotational–divergent propagation. It is unclear what a theory for this propagation might look like, but we expect it to be different from the divergent extension of the classical rotational theory discussed in appendix A due to the important role of heating. In this scenario of an internally determined divergence field, it is plausible that the divergence phase tilt could be affected by the mean meridional flow (e.g., through its impact on meridional propagation), which would explain our different conclusions from Kraucunas and Hartmann (2007) on the sensitivity of the eddy momentum fluxes to changes in the Hadley cell. It would be of interest to investigate what factors determine the divergence phase tilt in an idealized moist model similar to that of Shaw (2014), in which the divergence field is internally determined.

Although we have focused on the dominant stationary eddy momentum transport in this paper, similar constraints apply to propagating tropical modes in the corotating reference system, with implications for the latitudinal distribution of precipitation. A good example is the MJO. As shown in Part I, the MJO also produces divergent eddy momentum transport into the Northern (Southern) Hemisphere during JJA (DJF), even if this transport is much weaker than that by the climatological stationary wave (Lee 1999). The left panels of Fig. 9 show regressions of upper-level divergence and (u_r', v_d') wind vectors on the MJO indices of Adames et al. (2016) during November–March (NJDFM), June–September (JJAS), and the whole year. We have chosen for illustration the MJO phase for which the maximum velocity potential difference is found at 150°E, but results are similar for other phases.[3] For the annual regression we

[3] For the different MJO phases, these regressions are computed as linear combinations of the regressions on the leading velocity potential EOFs defining the MJO (Adames and Wallace 2014a; see also Part I).

observe the well-known MJO shallow-tail shape (e.g., Adames and Wallace 2014b), and subtle phase tilts are also apparent during the two solstices. These phase tilts become much more obvious for individual large-scale zonal components: the right panels of Fig. 9 shows the $k = 1$ contribution to the MJO regression and similar features can also be seen for $k = 2$ (not shown). No meridional coarse graining is necessary in this case. We observe a southwest-to-northeast tilt during NDJFM, consistent with cross-equatorial propagation of Rossby waves forced south of the equator, and a northwest-to-southeast tilt during JJAS, consistent with southward propagation of Rossby waves forced in the northern tropics. These phase tilts and the accompanying anomalous streamfunction patterns are reminiscent of those described in Figs. 7 and 8 for the climatological stationary wave during the same seasons. Interestingly, the shallow-tail shape found in the annual regression appears to result, at least in part, from the mix of the two seasonal signals, though there is also some hint of westward retraction of the NH divergence during NDJFM. Note that the swallowtail pattern, with divergence lines tilting westward away from the equator, is *not* consistent with the poleward propagation of Rossby waves forced at the equator, which would require the opposite tilt based on the arguments presented in this paper. For symmetric, equatorially forced variability, a mechanism involving the interaction between off-equatorial Rossby waves and the equatorial Kelvin wave might be more relevant for producing the observed eddy momentum flux (Showman and Polvani 2011; Zurita-Gotor and Held 2018).

To conclude, we note that the arguments presented in this paper are based on an inviscid closure of the vorticity balance. In this limit, we have shown that for long zonal waves the streamfunction minimum is shifted a quarter wavelength to the west of the maximum positive vorticity forcing. In the presence of friction we expect this phase shift to be reduced, with the vorticity maximum–streamfunction minimum catching up in phase with the vorticity forcing in the frictionally dominated limit. Friction may be due to cumulus mixing or represent the damping effect of transience and nonlinearity on vorticity. Whatever the source, friction is an essential ingredient to the Gill (1980) problem and is thought to be important for the tropical circulation more generally. Friction is responsible for instance for preventing the westward and eastward spreading of the Rossby and Kelvin components of the Gill response and confining zonally the response to localized heating. We have shown that friction is also necessary to prevent resonance in the presence of a strong Hadley cell. However, our results suggest that friction may only be needed at the small scales, at least during JJA, when the inviscid, large-scale vorticity balance can be closed linearly to reasonable accuracy.

Acknowledgments. We thank three anonymous reviewers for suggestions that improved the focus and the clarity of this manuscript. P.Z.-G. acknowledges financial support by Grant CGL2015-72259-EXP from the State Research Agency of Spain.

APPENDIX A

Divergent Eddy Momentum Flux in Unforced Propagation

Section 3 reviews the theory of unforced, barotropic Rossby wave propagation in the presence of a basic state with both zonal and meridional components: $U(y)$ and $V(y)$. This is a classical refraction problem, in which the wave changes its meridional wavenumber $l(y)$ according to the dispersion relation, Eq. (3), conserving its zonal wavenumber k and frequency due to the symmetries of the problem. As noted in section 3, stationary wave propagation requires that $U + (l/k)V$ remains positive, so that with easterly U propagation is only possible when $Vl > 0$. This implies that the rotational eddy momentum flux $\overline{u_r' v_r'} \sim -(1/2)kl|\hat{\psi}|^2$ is directed from the winter to the summer hemisphere (opposite to V), consistent with observations.

However, as noted in the introduction, this prediction only applies to the rotational eddy momentum flux while in observations the divergent component $\overline{u_r' v_d'}$ dominates. To estimate this component, we assume that the divergent circulation is constrained by adjustment to balance, similar to the ageostrophic extratropical circulation. Following Schubert et al. (2009), we use the balance condition:

$$gh' = f\psi', \tag{A1}$$

where h' is the shallow-water depth and f is allowed to vary with latitude. Substituting this expression into the (linearized) shallow-water continuity equation,

$$\partial_t h' + U\partial_x h' + V\partial_y h' + HD' = 0, \tag{A2}$$

we obtain

$$D' = -\frac{1}{f\lambda^2}(\partial_t \psi' + U\partial_x \psi' + V\partial_y \psi') - \frac{V}{\beta\lambda_\beta^4}\psi', \tag{A3}$$

where $\lambda = \sqrt{gH}/f$, $\lambda_\beta = (gH)^{1/4}/\sqrt{\beta}$, and H is the mean layer depth. For a plane-wave solution, $\psi' \sim \hat{\psi} e^{i(kx+ly-kct)}$, we can write

$$\widehat{v_d} = il\hat{\chi} = -\frac{il\hat{D}}{k^2 + l^2} = \frac{il}{K^2}\left[\frac{ik(U-c) + ilV}{f\lambda^2} + \frac{V}{\beta\lambda_\beta^4}\right]\hat{\psi}, \tag{A4}$$

where $K^2 = k^2 + l^2$ is the squared horizontal wavenumber.

Using $\widehat{u_r} = -il\hat{\psi}$ and the above expression for $\widehat{v_d}$ we finally obtain

$$\overline{u_r' v_d'} = \frac{1}{2}\mathrm{Re}\{\widehat{u_r}^* \widehat{v_d}\} = -\frac{Vl^2}{2\beta K^2 \lambda_\beta^4}|\hat{\psi}|^2, \tag{A5}$$

so that the divergent eddy momentum flux is also directed against the mean meridional flow V. Note that it is key for the above derivation to consider the latitudinal dependence of f, which produces the last term in Eqs. (A3) and (A4). Without this term, v_d' would be 180° out of phase with ψ' and in quadrature with u_r', and there would be no divergent momentum flux.

Using the dispersion relation, we can also estimate the ratio between both eddy momentum flux components:

$$\frac{\overline{u_r' v_r'}}{\overline{u_r' v_d'}} = K^4 \lambda_\beta^4 \left[1 + \frac{k(U-c)}{Vl}\right], \tag{A6}$$

suggesting that for long waves compared to the scale λ_β the divergent momentum flux becomes the dominant component to the full momentum flux, provided that the zonal wind is not too strong.

At first sight, this result seems consistent with the observations. Comparing the solid and dashed black lines in Fig. 1, we can see that the rotational and divergent contributions to the cross-equatorial stationary eddy momentum flux have the same sign through the seasonal cycle (see also Figs. 7 and 8 in Part I). However, while the divergent flux is strongly dominated by the $k = 1$ component (red dashed line), the rotational momentum flux by this wavenumber (red solid line) is negligible for all seasons but DJF, when its sign is opposite to that of $\overline{u_r' v_d'}$. The theory derived above might perhaps explain the $k = 2$–3 momentum flux contributions, but not the dominant $k = 1$ contribution.

As discussed in Part I, while the rotational momentum fluxes have an extratropical origin (they diverge through the tropics), the divergent momentum fluxes are associated with a region of strong momentum convergence/eddy generation adjacent to the equator in the summer hemisphere. The implication is that one cannot regard $\overline{u_r' v_d'}$ simply as a by-product of the rotational propagation as envisioned in this appendix: it is essential to consider the tropical heating to understand the determination of this flux. Adding a heating-term HQ' to the right-hand side of Eq. (A2), we now have $D' = Q' + D'_{\mathrm{ad}}$ where the adiabatic contribution D'_{ad} is defined by Eq. (A3). This contribution is in general much smaller than the heating. More importantly, the vorticity sources due to vortex stretching and divergent vorticity advection can no longer be neglected in the vorticity equation.

APPENDIX B

Divergent Momentum Flux Response When the Rotational Tendency Is Dominated by β

In this limit, the vorticity balance reduces to

$$ik\beta\tilde{\psi} = \tilde{F}, \tag{B1}$$

where tildes are used to indicate that the Fourier transform is only taken in the zonal direction: $\tilde{\psi} = f(k, y)$. Differentiating this expression meridionally, we obtain

$$\tilde{u}_r = -\tilde{\psi}_y = \frac{i\tilde{F}_y}{\beta k} \tag{B2}$$

and a divergent momentum flux:

$$\overline{u_r' v_d'} = \frac{1}{2}\mathrm{Re}\{\tilde{u}_r \tilde{v}_d^*\} = -\frac{1}{2\beta k}\mathrm{Im}\{\tilde{F}_y \tilde{v}_d^*\}. \tag{B3}$$

Expressing $\tilde{v}_d = R(y)\exp\{i[kx + \Theta(y)]\}$, where R is the amplitude and Θ the phase of the divergent meridional velocity, we can calculate the momentum flux response to meridional divergent advection ($\tilde{F} = -\beta\tilde{v}_d$) as

$$\overline{u_r' v_d'}^{\beta} = \frac{R^2\Theta_y}{2k}, \tag{B4}$$

whose sign only depends on the tilt of the phase lines consistent with Eq. (7).

To calculate the response to vortex stretching, we differentiate $\tilde{F} = -f\tilde{D} = -f(ik\tilde{u}_d + \tilde{v}_{dy})$:

$$\tilde{F}_y = -ik\beta\tilde{u}_d - \beta\tilde{v}_{dy} + fk^2\tilde{v}_d - f\tilde{v}_{dyy}, \tag{B5}$$

where we took into account that $\tilde{u}_d$ and $\tilde{v}_d$ are irrotational, so that $\tilde{u}_{dy} = ik\tilde{v}_d$. Plugging into Eq. (B3), the first term gives $\overline{u_d' v_d'}$, the second term gives $\overline{u_r' v_d'}^{\beta}$, and the third term vanishes. Finally, the last term can be expressed as

$$\begin{aligned}\frac{1}{2\beta k}\mathrm{Im}\{f\tilde{v}_{dyy}\tilde{v}_d^*\} &= \frac{f}{2\beta k}\mathrm{Im}\{\partial_y(\tilde{v}_{dy}\tilde{v}_d^*) - \tilde{v}_{dy}\tilde{v}_{dy}^*\} \\ &= \frac{f}{\beta}\frac{\partial}{\partial y}(\overline{u_r' v_d'}^{\beta}),\end{aligned} \tag{B6}$$

so that the full eddy momentum flux response is given by

$$\overline{u_r' v_d'}^{\mathrm{str}} \approx \overline{u_r' v_d'}^{\beta} + \frac{f}{\beta}\frac{\partial}{\partial y}(\overline{u_r' v_d'}^{\beta}), \tag{B7}$$

where we neglected $\overline{u_d'v_d'}$ (see Part I). Equation (B7) implies that $\overline{u_r'v_d'}^{\beta}$ and $\overline{u_r'v_d'}^{\text{str}}$ must have the same sign when $\overline{u_r'v_d'}^{\beta} = R^2\Theta_y/2k$ varies more slowly than f, which is consistent with our findings in section 3 (although the observed divergence field has fine meridional structure, the eddy momentum flux is dominated by the gravest modes of this field).

If $\overline{u_r'v_d'}^{\beta}$ were constant with latitude, the response to vortex stretching would double up the momentum flux forced by the divergent meridional advection. The additional enhancement in the momentum flux is associated with the meridional structure of $\overline{u_r'v_d'}^{\beta}$. When $\partial_y(\overline{u_r'v_d'}^{\beta}) < 0$, this term produces a positive (negative) contribution to $\overline{u_r'v_d'}^{\text{str}}$ in the Southern (Northern) Hemisphere, hence an equatorward momentum flux in both hemispheres. During the solstice seasons, when the eddy forcing and eddy momentum convergence move into the summer hemisphere, this contribution weakens the momentum flux directed from the equator to the forcing latitude in the summer hemisphere and strengthens the equatorward momentum flux in the winter hemisphere. Although this seems qualitatively consistent with the seasonal cycle in Fig. 2, Eq. (B7) does not work well quantitatively (not shown), presumably because Eq. (B1) is not a good approximation when $\overline{u_r'v_d'}^{\beta}$ has meridional structure.

REFERENCES

Adames, Á. F., and J. M. Wallace, 2014a: Three-dimensional structure and evolution of the MJO and its relation to the mean flow. *J. Atmos. Sci.*, **71**, 2007–2026, https://doi.org/10.1175/JAS-D-13-0254.1.

——, and ——, 2014b: Three-dimensional structure and evolution of the vertical velocity and divergence fields in the MJO. *J. Atmos. Sci.*, **71**, 4661–4681, https://doi.org/10.1175/JAS-D-14-0091.1.

——, ——, and J. M. Monteiro, 2016: Seasonality of the structure and propagation characteristics of the MJO. *J. Atmos. Sci.*, **73**, 3511–3526, https://doi.org/10.1175/JAS-D-15-0232.1.

Adler, R. F., and Coauthors, 2003: The version-2 Global Precipitation Climatology Project (GPCP) monthly precipitation analysis (1979–present). *J. Hydrometeor.*, **4**, 1147–1167, https://doi.org/10.1175/1525-7541(2003)004<1147:TVGPCP>2.0.CO;2.

Arnold, N. P., E. Tziperman, and B. Farrell, 2012: Abrupt transition to strong superrotation driven by equatorial wave resonance in an idealized GCM. *J. Atmos. Sci.*, **69**, 626–640, https://doi.org/10.1175/JAS-D-11-0136.1.

Dee, D. P., and Coauthors, 2011: The Era-Interim reanalysis: Configuration and performance of the data assimilation system. *Quart. J. Roy. Meteor. Soc.*, **137**, 553–597, https://doi.org/10.1002/qj.828.

Dima, I. M., J. M. Wallace, and I. Kraucunas, 2005: Tropical zonal momentum balance in the NCEP reanalyses. *J. Atmos. Sci.*, **62**, 2499–2513, https://doi.org/10.1175/JAS3486.1.

Gill, A., 1980: Some simple solutions for heat-induced tropical circulation. *Quart. J. Roy. Meteor. Soc.*, **106**, 447–462, https://doi.org/10.1002/qj.49710644905.

Hoskins, B. J., and D. J. Karoly, 1981: The steady linear response of a spherical atmosphere to thermal and orographic forcing. *J. Atmos. Sci.*, **38**, 1179–1196, https://doi.org/10.1175/1520-0469(1981)038<1179:TSLROA>2.0.CO;2.

——, and T. Ambrizzi, 1993: Rossby wave propagation on a realistic longitudinally varying flow. *J. Atmos. Sci.*, **50**, 1661–1671, https://doi.org/10.1175/1520-0469(1993)050<1661:RWPOAR>2.0.CO;2.

——, R. Neale, M. Rodwell, and G.-Y. Yang, 1999: Aspects of the large-scale tropical atmospheric circulation. *Tellus*, **51B**, 33–44, https://doi.org/10.3402/tellusb.v51i1.16258.

Kraucunas, I., and D. L. Hartmann, 2007: Tropical stationary waves in a nonlinear shallow-water model with realistic basic states. *J. Atmos. Sci.*, **64**, 2540–2557, https://doi.org/10.1175/JAS3920.1.

Lee, S., 1999: Why are the climatological zonal winds easterly in the equatorial upper troposphere? *J. Atmos. Sci.*, **56**, 1353–1363, https://doi.org/10.1175/1520-0469(1999)056<1353:WATCZW>2.0.CO;2.

Li, Y., J. Li, F. F. Jin, and S. Zhao, 2015: Interhemispheric propagation of stationary Rossby waves in a horizontally nonuniform background flow. *J. Atmos. Sci.*, **72**, 3233–3256, https://doi.org/10.1175/JAS-D-14-0239.1.

Monteiro, J. M., A. F. Adames, J. M. Wallace, and J. S. Sukhatme, 2014: Interpreting the upper level structure of the Madden-Julian oscillation. *Geophys. Res. Lett.*, **41**, 9158–9165, https://doi.org/10.1002/2014GL062518.

Sardeshmukh, P. D., and B. J. Hoskins, 1985: Vorticity balances in the tropics during the 1982-83 El Niño-Southern Oscillation event. *Quart. J. Roy. Meteor. Soc.*, **111**, 261–278, https://doi.org/10.1256/smsqj.46801.

——, and ——, 1988: The generation of global rotational flow by steady idealized tropical divergence. *J. Atmos. Sci.*, **45**, 1228–1251, https://doi.org/10.1175/1520-0469(1988)045<1228:TGOGRF>2.0.CO;2.

Schneider, E. K., and I. G. Watterson, 1984: Stationary Rossby wave propagation through easterly layers. *J. Atmos. Sci.*, **41**, 2069–2083, https://doi.org/10.1175/1520-0469(1984)041<2069:SRWPTE>2.0.CO;2.

Schubert, W. H., R. K. Taft, and L. G. Silvers, 2009: Shallow water quasi-geostrophic theory on the sphere. *J. Adv. Model. Earth Syst.*, **1** (2), https://doi.org/10.3894/JAMES.2009.1.2.

Shaw, T. A., 2014: On the role of planetary-scale waves in the abrupt seasonal transition of the Northern Hemisphere general circulation. *J. Atmos. Sci.*, **71**, 1724–1746, https://doi.org/10.1175/JAS-D-13-0137.1.

Showman, A. P., and L. M. Polvani, 2011: Equatorial superrotation on tidally locked exoplanets. *Astrophys. J.*, **738**, 71, https://doi.org/10.1088/0004-637X/738/1/71.

Webster, P. J., and J. R. Holton, 1982: Cross-equatorial response to middle-latitude forcing in a zonally varying basic state. *J. Atmos. Sci.*, **39**, 722–733, https://doi.org/10.1175/1520-0469(1982)039<0722:CERTML>2.0.CO;2.

Yang, G.-Y., and B. J. Hoskins, 2017: The equivalent barotropic structure of waves in the tropical atmosphere in the Western Hemisphere. *J. Atmos. Sci.*, **74**, 1689–1704, https://doi.org/10.1175/JAS-D-16-0267.1.

Zurita-Gotor, P., 2019: The role of the divergent circulation for large-scale eddy momentum transport in the tropics. Part I: Observations. *J. Atmos. Sci.*, **76**, 1125–1144, https://doi.org/10.1175/JAS-D-18-0297.1.

——, and P. Álvarez-Zapatero, 2018: Coupled interannual variability of the Hadley and Ferrel cells. *J. Climate*, **31**, 4757–4773, https://doi.org/10.1175/JCLI-D-17-0752.1.

——, and I. M. Held, 2018: The finite-amplitude evolution of mixed Kelvin–Rossby wave instability and equatorial superrotation in a shallow-water model and an idealized GCM. *J. Atmos. Sci.*, **75**, 2299–2316, https://doi.org/10.1175/JAS-D-17-0386.1.